ORIENTAL JOURNAL OF CHEMISTRY
An International Open Access, Peer Reviewed Research Journal
www.orientjchem.org
ISSN: 0970-020 X
CODEN: OJCHEG
2024, Vol. 40, No.(6):
Pg. 1578-1588

Effect of Calcium nitrite and Nano TiO_2 Admixed Cement Slurry Coatings on Corrosion of Steel

MD DANIYAL[1]*, MADAN KUMAR[3], UBAIDURRAHMAN ANSARI[2], VIJAY KUMAR[4] and RAHUL KUMAR[1]

[1]Department of Civil Engineering, Sandip University, Sijoul, Madhubani, India.
[3]Department of Civil Engineering, Government Polytechnic, Muzaffarpur, India.
[2]Department of Civil Engineering, SND College of Engineering and Research Centre, Yeola, India.
[4]Department of Civil Engineering, Muzaffarpur Institute of Technology, Muzaffarpur, India.
*Corresponding author E-mail: daniyalzhcet@gmail.com

http://dx.doi.org/10.13005/ojc/400608

(Received: October 07, 2024; Accepted: December 01, 2024)

ABSTRACT

The corrosion control mechanisms of ordinary Portland cement (OPC) slurry-coated, calcium nitrite admixed OPC slurry-coated and nano-TiO_2 admixed OPC slurry-coated steel under normal water and saline water (3.5% NaCl) exposure were investigated. To estimate the corrosion rate of coating systems, the potentiodynamic polarization measurements were performed after 30, 60, 90, and 120 days of exposure in normal and saline environments. The weight loss measurements at the exposure duration of 120 days were also carried out to validate the results of potentiodynamic polarization measurements. Moreover, setting time and compressive strength were also determined to assess the impact of calcium nitrite and nano-TiO_2 on the quality of cementitious composite. The results revealed that all the coating systems showed a significant degree of corrosion inhibition as compared to bare steel. The calcium nitrite and nano-TiO_2 admixed cement slurry-coated steel showed higher corrosion inhibition efficiency than OPC slurry-coated steel.

Keywords: Corrosion rate, Calcium nitrite, Nano-TiO_2, Potentiodynamic polarization measurements, Weight loss measurements.

INTRODUCTION

Steel-reinforced concrete is widely regarded as an ideal construction material, making it a popular choice for building structures. This choice is a result of the material's unique properties, which include remarkable compressive strength from concrete and significant tensile strength from steel reinforcement. When combined, these qualities provide a robust and adaptable material that can withstand a variety of structural demands. Normally embedded steel in the composite is in a passive condition against corrosion owing to a highly stable and insoluble thin iron oxide film (γ-$Fe_2O_3.H_2O$) which is formed on the steel surface in the extremely alkaline environment of concrete pore solution (pH=12.5-13). However, this protective layer can be destroyed when exposed

to hostile environments like high Carbon dioxide or chloride ions (admixtures containing chloride, seawater, unwashed sea sand, de-icing salt etc.) concentration. The interaction of CO_2 with pore water (H_2O) and $Ca(OH)_2$ yields calcium carbonate, diminishing concrete alkalinity (Eq.1, Eq. 2). Simultaneously, chloride ions permeate micro-pores of concrete, accumulating on steel surfaces, thereby destroying its protective film (Eq.3, Eq.4)[1-5].

$$CO_2 + H_2O \longrightarrow H_2CO_3 \quad (1)$$

$$H_2CO_3 + Ca(OH)_2 \longrightarrow CaCO_3 + 2H_2O \quad (2)$$

$$Fe^{2+} + 2Cl^- \longrightarrow FeCl_2 \quad (3)$$

$$FeCl_2 + 2H_2O \longrightarrow Fe(OH)_2 + 2HCl \quad (4)$$

Once the corrosion of steel begins, the propagation of corrosion increases and consequently produces the large amount of rust which have about 3-8 times greater volume than the original steel. This causes pressure on the concrete resulting cracking as well as spalling of the cover concrete, which further speeds up the corrosion process. This process is continued till the entire reinforced concrete structure deteriorated[6]. Steel corrosion is fundamentally an electrochemical process where different regions of the steel serve as anodes and cathodes, while the moisture (pore solution) available in the cementitious composites functions as the electrolyte. At anode, loss of electrons occurs which moves through steel to the cathodic site and then reacts with oxygen and water at the cathode and thus produces hydroxide ions, which move through the electrolyte to the anodic site. This mechanism initiates a redox reaction, as illustrated in Eq.(5) and Eq.(6)[7].

$$2Fe \longrightarrow 2Fe^{2+} + 4e^- \quad (5)$$

$$4e^- + 2H_2O + O_2 \longrightarrow 4OH^- \quad (6)$$

By regulating one of these reactions, the corrosion process can be effectively managed. Additionally, several strategies can be employed to prevent or mitigate corrosion of embedded steel. These include selecting corrosion-resistant steel, applying protective coatings, using concrete sealers, increasing concrete cover thickness, incorporating supplementary cementitious materials, adding corrosion inhibitors, and implementing cathodic protection. Since 1970, calcium nitrite has primarily been utilized as a corrosion inhibitor in reinforced cementitious composites. In fact, calcium nitrite is an anodic inhibitor, which reacts with ferrous ions (Fe^{2+}) at the anode and forms a ferric oxide (Fe_2O_3) film on the surface of steel as shown in Eq.(7) and Eq.(8). Further, calcium nitrite ions react with the ferrous ions more rapidly compared to the chloride ions and form a more stable passive layer (γ-FeOOH), thus increase the corrosion resistance properties of steel[8-10].

$$2Fe^{2+} + 2OH^- + 2NO^{2-} \longrightarrow 2NO + Fe_2O_3 + H_2O \quad (7)$$

$$Fe^{2+} + OH^- + NO^{2-} \longrightarrow NO + \gamma\text{-FeOOH} \quad (8)$$

Recently, nano-TiO_2 have attracted significant attention in the construction industry for their self-cleaning properties and ability to remove air pollutants through photocatalytic reactions[11]. Additionally, studies show that incorporating the right amount of nano-TiO_2 enhances the desirable properties of cementitious composites. This improvement is largely due to the ultra-fine nature of nano-TiO_2 particles, which not only fill micro-voids within the composite but also act as nucleation sites, reducing the size of $Ca(OH)_2$ crystals and accelerating the hydration process. This leads to greater consumption of $Ca(OH)_2$ and the formation of an increased amount of C-S-H gel, significantly boosting the overall performance cementitious composites[12-16].

This study evaluates the effectiveness of various protective coatings such as cement slurry, calcium nitrite-admixed cement slurry, and nano-TiO_2-admixed cement slurry in mitigating steel corrosion. Various corrosion kinetic parameters of specimens were obtained by conducting potentiodynamic polarization test after 30, 60, 90, and 120 days of exposure to both normal and saline environments. The weight loss measurements at the exposure duration of 120 days were also performed in order to validate the results of potentiodynamic polarization measurements. Each category of specimens was tested in triplicate to ensure reliable results.

MATERIALS AND METHODOLOGY

Materials

In this investigation, 43-grade ordinary

Portland cement (OPC), calcium nitrite with a minimum purity of 98%, nano-TiO_2 with 30nm particle size, and mild steel bars of 3mm diameter were utilized. The exposure environments included tap water with a pH of 7.2 and saline water (3.5% NaCl solution) with a pH of 7.3.

SEM and EDX Analysis

A Scanning Electron Microscope (SEM) is a powerful imaging tool that uses a focused beam of high-energy electrons to examine the surface of a sample at very high magnifications. When the electron beam interacts with the sample, it generates signals in the form of secondary electrons, backscattered electrons, and X-rays. These signals provide detailed information about the sample's surface topography, texture, and composition. SEM can produce three-dimensional images with a high depth of field, making it ideal for analysing microstructures, fractures, and surface coatings. Energy-Dispersive X-ray Spectroscopy (EDX) is often coupled with SEM to analyze the elemental composition of a material. When the electron beam from the SEM strikes the sample, it excites the atoms, causing them to emit characteristic X-rays. Each element emits X-rays at unique energy levels, allowing for the identification and quantification of the elements present in the sample.

In this study, the microstructural characteristics and elemental compositions of all the materials were analyzed using SEM and EDX techniques, respectively. The SEM micrograph of OPC, shown in Fig. 1, reveals rough surfaces with irregular shapes and sizes. This irregularity indicates potential for filling the gaps between OPC particles with finer materials. This possibly will lead to improvement in the microstructural properties of OPC. Moreover, the elemental composition of OPC is shown in Figure 2.

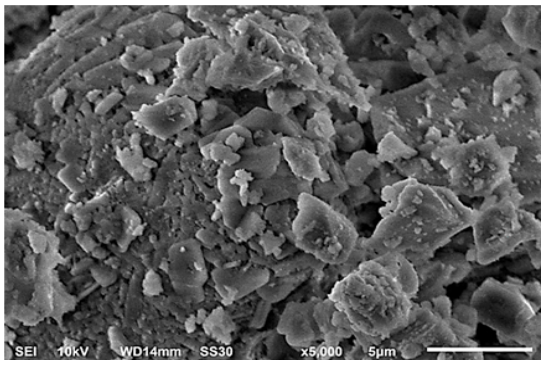

Fig. 1. SEM micrograph of unhydrated OPC

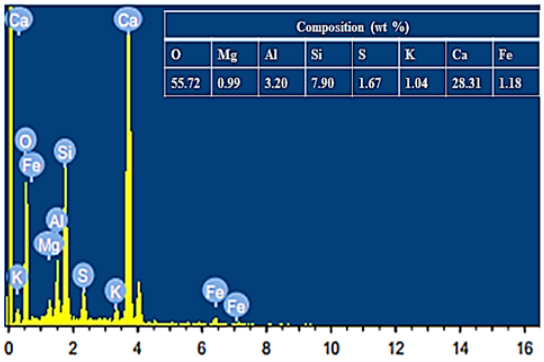

Fig. 2. EDX spectrum and EDX analysis results of unhydrated OPC

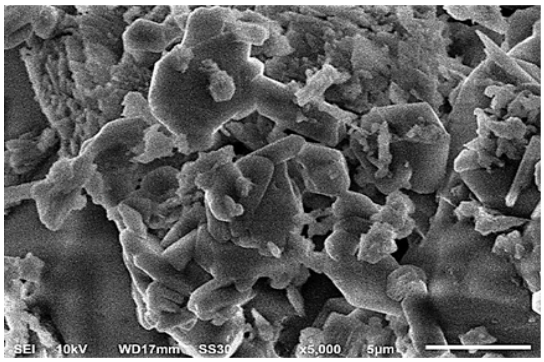

Fig. 3. SEM micrograph of calcium nitrite

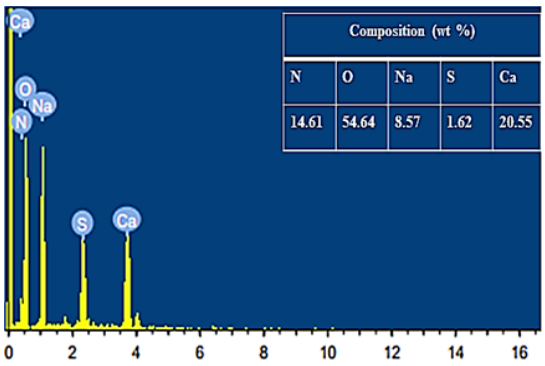

Fig. 4. EDX spectrum and EDX analysis results of calcium nitrite

The SEM and EDX analysis of calcium nitrite was conducted and their respective plots can be seen in Fig. 3 and Fig. 4. Besides, density and melting point of calcium nitrite as provided by the supplier was 2.26 g/cm^3 and 390°C respectively. It has also been observed that the calcium nitrite is highly soluble in water. The SEM image and EDX spectrum of nano-TiO_2 are shown in Fig. 5 and Fig. 6, respectively. The average particle size of nano-TiO_2 was observed to be 30nm. The SEM image of steel is shown in Fig. 7 and the corresponding EDX spectra and its results are shown in Figure 8.

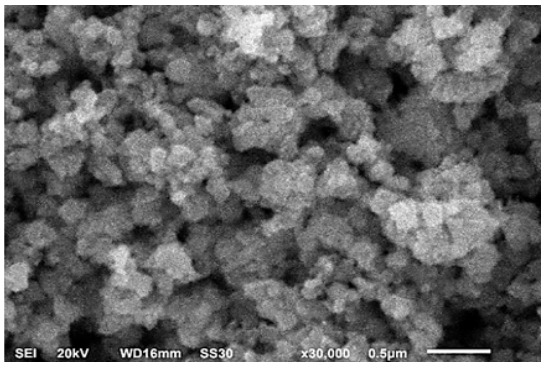

Fig. 5. SEM micrograph of nano-TiO_2

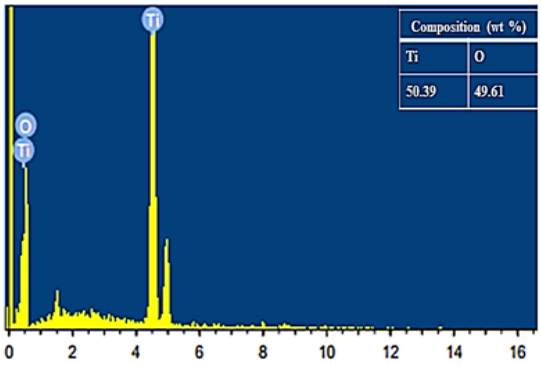

Fig. 6. EDX spectrum and EDX analysis results of nano-TiO_2

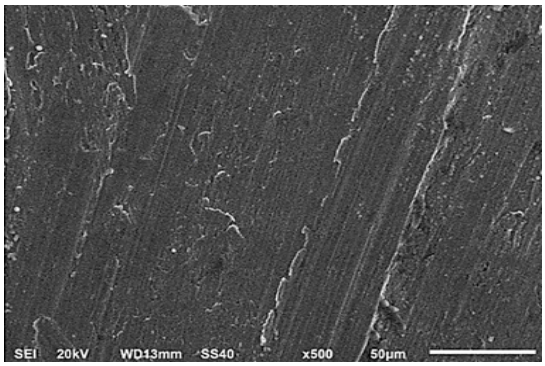

Fig. 7. SEM micrograph of mild steel

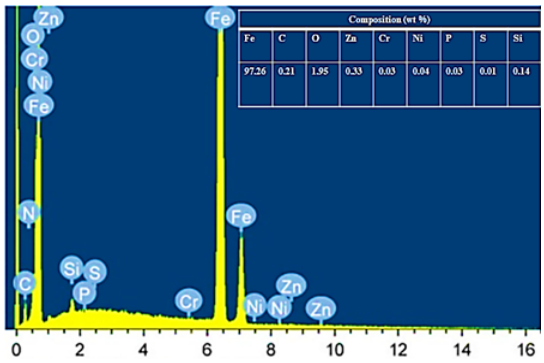

Fig. 8. EDX spectrum and EDX analysis results of mild steel

Test Specimens and Methods

Mix proportion of Slurry Coatings

Seven types of coatings were prepared namely ordinary Portland cement (OPC) slurry coating (SC), cement slurry containing 1% (CN1), 3% (CN3) and 5% (CN5) calcium nitrite (CN); and 1% (TO1), 3% (TO3) and 5% (TO5) nano-TiO_2 (TO) by weight of cement.

To prepare the coatings, OPC was first mixed with water at a fixed ratio (w/c=0.5) and stirred for 3 minutes. Then, varying percentages of CN or TO were gradually added to the cement slurry, followed by stirring for an additional 5 min using a magnetic stirrer. The resulting mixtures were then applied to the steel surfaces and left to air dry for 24 hours. Also, bare steel (BS) specimens of the same size were prepared for comparison. Thereafter, all the specimens were kept in exposure environments for 120 days as shown in Figure 9.

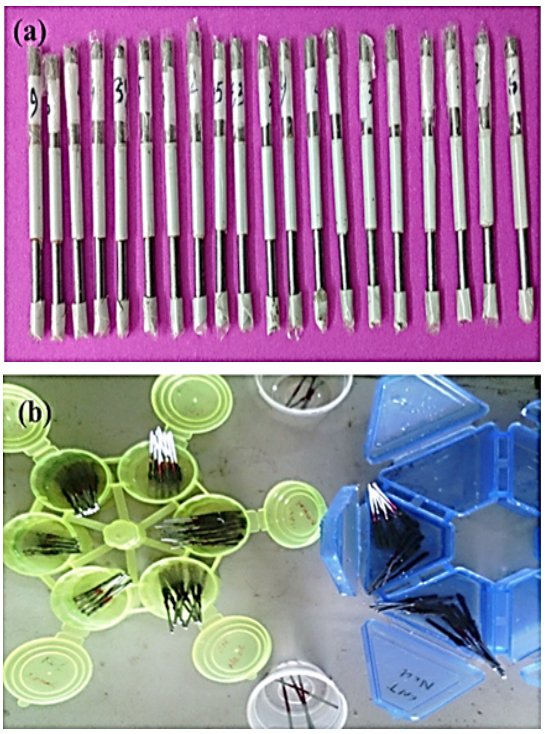

Fig. 9(a). Specimen before coating and (b) Coated specimens exposed to environment

Potentiodynamic Polarization Measurements

The Gill AC Potentiostat was used to conduct potentiodynamic polarization test. The experiment utilized a standard three-electrode electrochemical cell setup, where the specimens acted as the working electrodes (WE). A

saturated calomel electrode (SCE) served as the reference electrode (RE), while a platinum electrode was used as the counter electrode (CE). Additionally, a working sense (WS) was connected to the working electrode to measure the potential. For comparison, both normal water (NW) and saline water (SW) were used as the electrolyte in the cell. In this setup, the WE and CE carried the current, while the WS and RE measured the potential[17,18].

A schematic diagram of the test specimen, test setup and ACM instrument during test is shown in Fig. 10(a), (b) and (c), respectively.

Potentiodynamic polarization measurements were conducted at 30, 60, 90, and 120-day intervals, starting with a potential of -250mV and reversing at 250mV, with a scan rate of 200mV/minute. The polarization curves obtained from the tests were analyzed by Tafel extrapolation technique to evaluate anodic and cathodic Tafel slopes (βa, βc), corrosion potential (E_{corr}), corrosion current density (I_{corr}), and corrosion rate (CR). Afterward, the inhibition efficiency (IE) of different percentage of admixtures was calculated using the following formula:

$$IE\ (\%) = \frac{(CR)o-(CR)i}{(CR)o} X100 \quad (9)$$

Here, $(CR)_o$ represents the corrosion rate of the bare or uninhibited steel, while $(CR)_i$ denotes the corrosion rate of the inhibited or admixed coated steel.

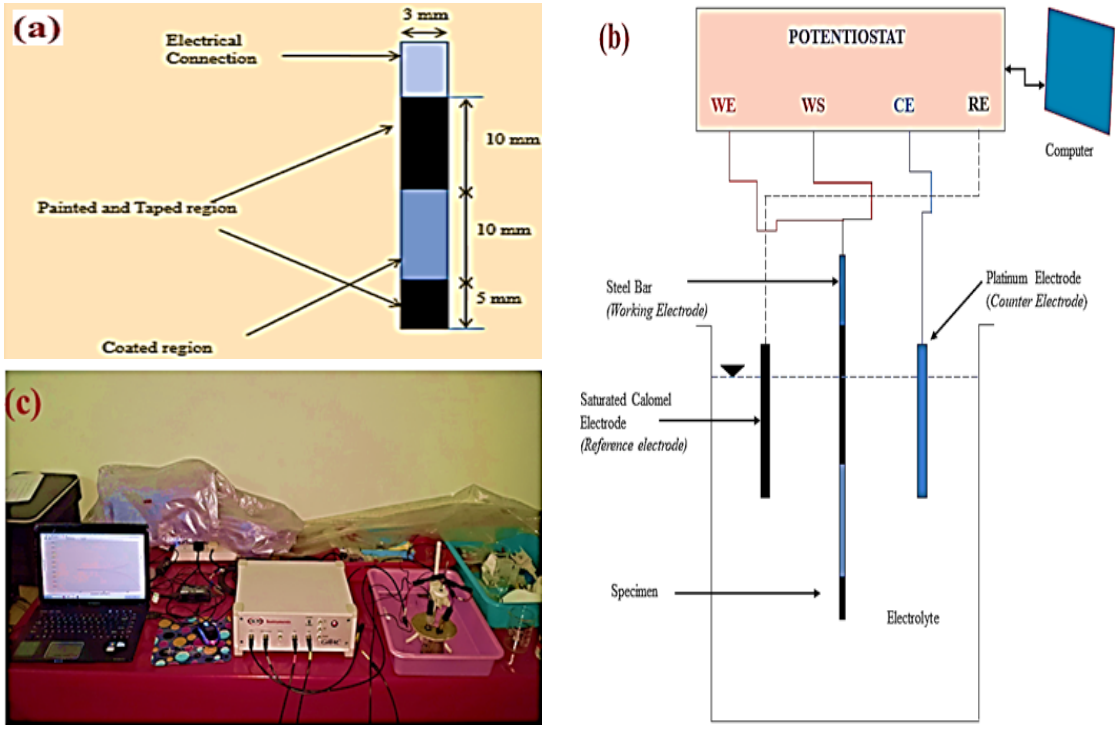

Fig. 10. Schematic diagram of (a) test specimen (b) test setup and (c) ACM instrument

Weight Loss Measurements

To validate the results of the potentiodynamic polarization measurements, weight loss tests were conducted according to ASTM G1-90 standards after a 120-day exposure period. The mild steel specimens were weighed using digital weighing balance after the removal of coatings and other deposits. The weight loss was determined by subtracting the final weight of the specimens from their initial weight. Afterward, the CR in mpy (mils per year) was calculated using the formula[19-21]:

$$CR\ (mpy) = (K \times W)/(D \times A \times T) \quad (10)$$

Where: K = Constant (3.45×10^6), W = Mass Loss (grams), D = Density (g/cm^3), A = Exposed Area (cm^2), T= Exposure Time (hours)

RESULTS AND DISCUSSION

This section presents the results of Potentiodynamic polarization measurements and Weight loss measurements of specimens exposed under normal water (NW) and saline water (SW).

Potentiodynamic polarization measurements of specimens exposed under normal water

Figures 11 through 18 display the cell potential vs. current density plots (polarization curves) for bare steel, cement slurry-coated, calcium nitrite-admixed cement slurry-coated, and nano-TiO_2-admixed cement slurry-coated specimens, all exposed to normal water for 30, 60, 90, and 120 days. The corrosion kinetic parameters, derived from analyzing the polarization curves, are summarized in Table 1. The data reveal that corrosion current density increased with longer exposure durations for all samples. However, a notable decrease in corrosion current density was observed with higher concentrations of calcium nitrite and nano-TiO_2. The corresponding corrosion rate and inhibition efficiency of all the coating systems with respect to the bare steel were also calculated and given in the Table 1.

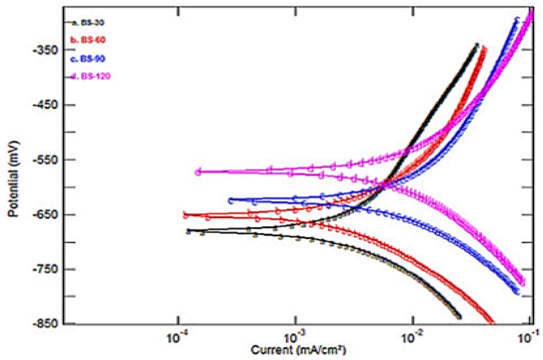

Fig. 11. Polarization curves of BS exposed under NW

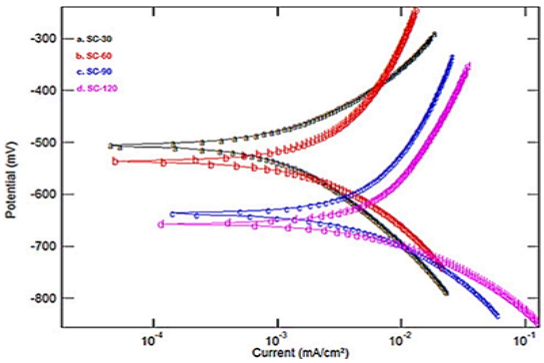

Fig. 12. Polarization curves of SC exposed under NW

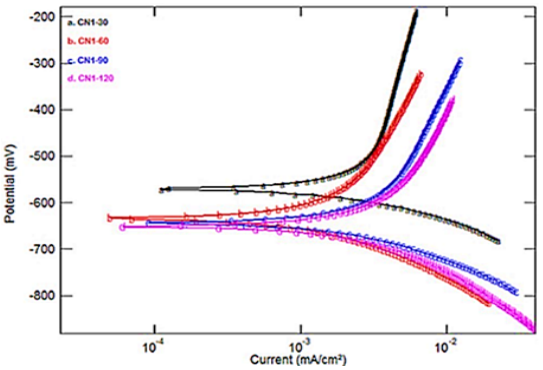

Fig. 13. Polarization curves of CN1 exposed under NW

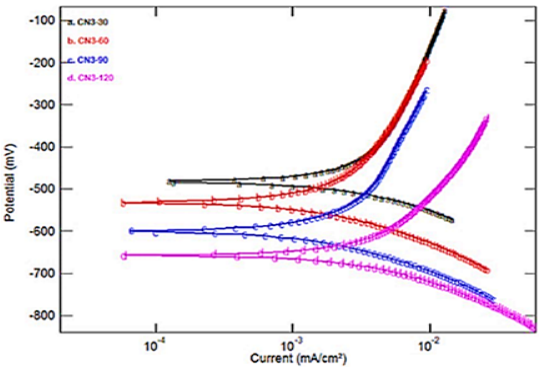

Fig. 14. Polarization curves of CN3 exposed under NW

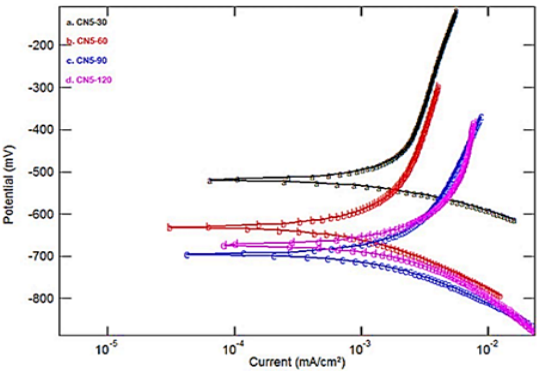

Fig. 15. Polarization curves of CN5 exposed under NW

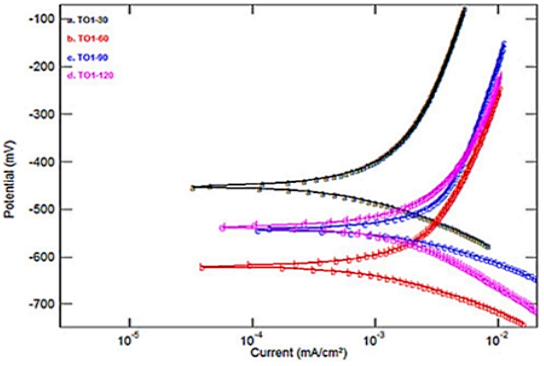

Fig. 16. Polarization curves of TO1 exposed under NW

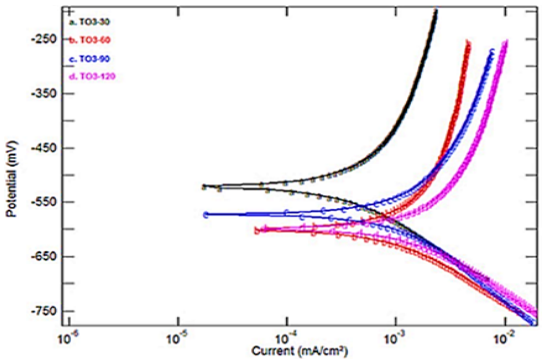

Fig. 17. Polarization curves of TO3 exposed under NW

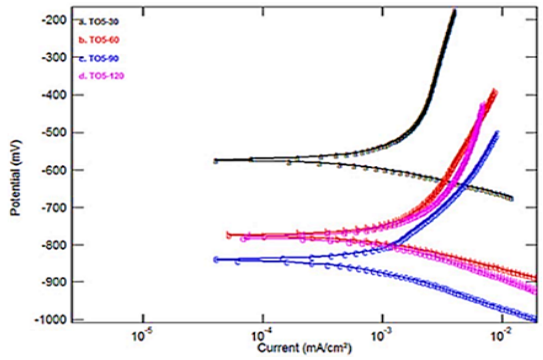

Fig. 18. Polarization curves of TO5 exposed under NW

Table 1: Corrosion kinetic parameters of specimens exposed under NW

System with Duration	E_{corr} (mV)	I_{corr}(mA/cm^2)	CR(mils/yr.)	IE (%)
BS-30	-680.05	0.0027899	1.273000	-
SC-30	-506.43	0.0010642	0.498216	60.86
CN1-30	-573.35	0.0009564	0.436420	65.72
CN3-30	-482.21	0.0007864	0.364520	71.37
CN5-30	-519.51	0.0004136	0.162414	87.24
TO1-30	-451.65	0.0006133	0.279827	78.02
TO3-30	-521.66	0.0004654	0.212342	83.32
TO5-30	-572.58	0.0003946	0.148310	88.35
BS-60	-651.16	0.0065102	2.970600	-
SC-60	-537.12	0.0025709	1.173000	60.51
CN1-60	-633.64	0.0016883	0.770377	74.07
CN3-60	-531.38	0.0016253	0.741618	75.03
CN5-60	-629.80	0.0009793	0.442475	85.10
TO1-60	-616.46	0.0010599	0.483633	83.72
TO3-60	-600.98	0.0010333	0.471487	84.13
TO5-60	-772.17	0.0007850	0.358185	87.94
BS-90	-623.44	0.0103696	4.731600	-
SC-90	-639.00	0.0049050	2.238100	52.70
CN1-90	-643.45	0.0022404	1.022200	78.40
CN3-90	-600.54	0.0017864	0.815118	82.77
CN5-90	-695.05	0.0015663	0.714720	84.89
TO1-90	-539.46	0.0016950	0.719036	84.80
TO3-90	-571.82	0.0014854	0.676541	85.70
TO5-90	-839.26	0.0012854	0.586541	87.60
BS-120	-571.45	0.0139845	6.381100	-
SC-120	-657.42	0.0056498	2.577900	59.60
CN1-120	-651.87	0.0039066	1.813200	71.58
CN3-120	-657.39	0.0035134	1.603100	74.88
CN5-120	-671.75	0.0025564	1.103100	82.71
TO1-120	-534.05	0.0026027	1.150700	81.97
TO3-120	-599.80	0.0020581	0.947859	85.15
TO5-120	-777.20	0.0015385	0.810745	87.29

All the coating systems show considerable level of corrosion inhibition efficiency. For example, IE of SC, CN5 and TO5 with respect to the BS, at the exposure duration of 30, 60, 90 and 120 days were found as 60.86%, 60.51%, 52.70% and 59.60%; 87.24%, 85.10%, 84.89% and 82.71%; 88.35%, 87.94 %, 87.60% and 87.29% respectively. Interestingly, the incorporation of calcium nitrite and nano-TiO_2 significantly enhanced the inhibition efficiency of the plain cement slurry coating system. For instance, the IE of CN5 with respect to the SC, at the exposure duration of 30, 60, 90 and 120 days were found as 67.41%, 62.28%, 68.07% and 52.21% respectively; and the corrosion inhibition efficiency of TO5 with respect to the SC, at the exposure duration of 30, 60, 90 and 120 days were found as 70.23%, 69.46 %, 73.79% and 68.55% respectively. Moreover, the effectiveness of CN5 and TO5 as compared to BS and SC after 120 days exposure can be clearly seen in the Figure 19.

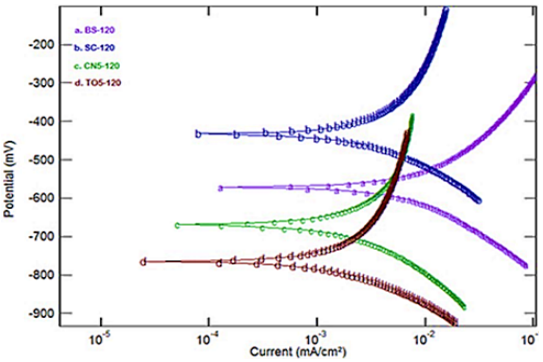

Fig. 19. Polarization curve of BS, SC, CN5 and TO5 systems exposed under NW for 120 days

Potentiodynamic Polarization Measurements of specimens exposed under saline water

Figures 20 through 27 illustrate the polarization curves for bare steel, cement slurry-coated, calcium nitrite-admixed cement slurry-coated, and nano-TiO_2-admixed cement slurry-coated specimens exposed to saline water for 30, 60, 90, and 120 days. The corrosion kinetic parameters are detailed in Table 2. The results indicate that corrosion current density increased for all samples with extended exposure time. Additionally, an increase in the concentrations of calcium nitrite and nano-TiO_2 resulted in a reduction of corrosion current density. The corresponding corrosion rate and inhibition efficiency of all the coating systems with respect to the bare steel were also calculated and given in the Table 2.

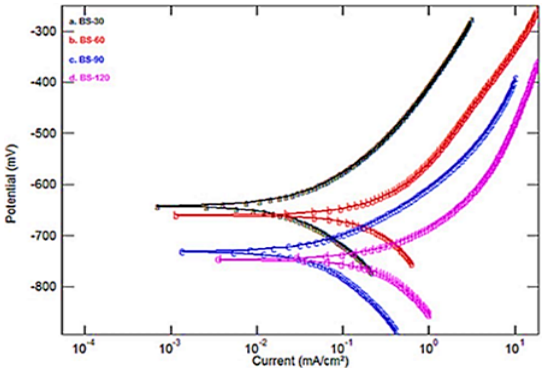

Fig. 20. Polarization curves of BS exposed under SW

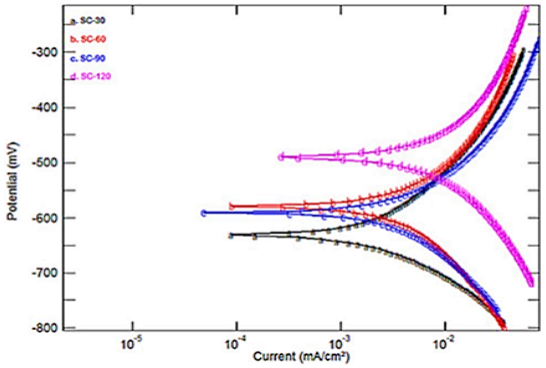

Fig. 21. Polarization curves of SC exposed under SW

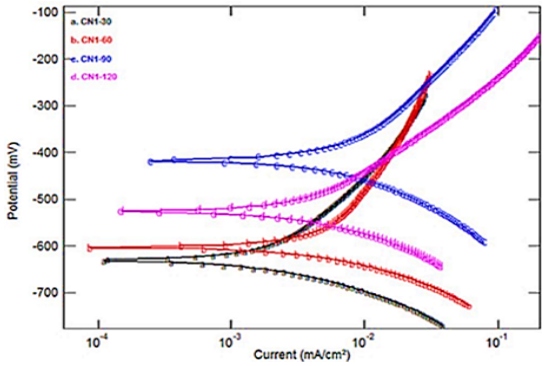

Fig. 22. Polarization curves of CN1 exposed under SW

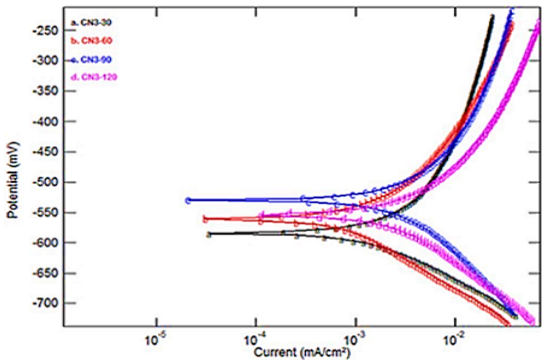

Fig. 23. Polarization curves of CN3 exposed under SW

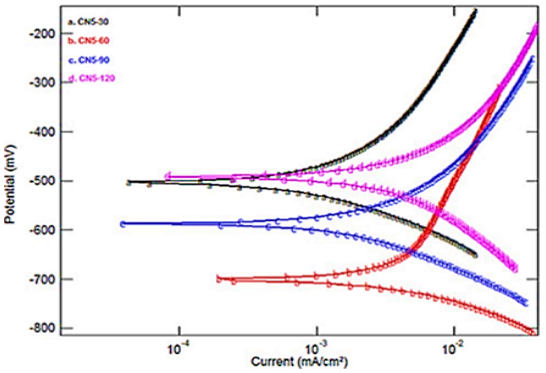

Fig. 24. Polarization curves of CN5 exposed under SW

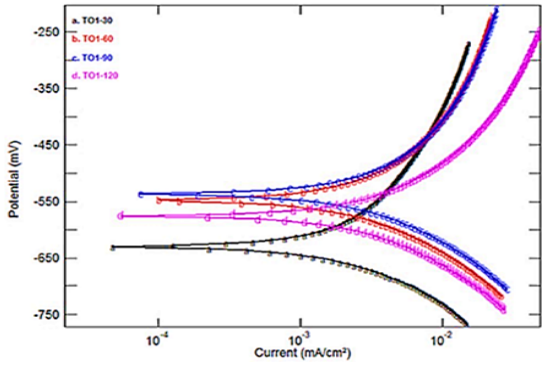

Fig. 25. Polarization curves of TO1 exposed under SW

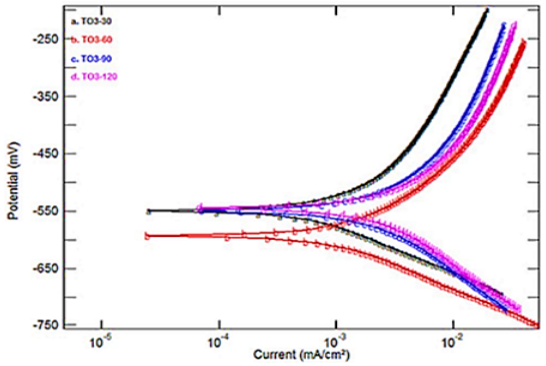

Fig. 26. Polarization curves of TO3 exposed under SW

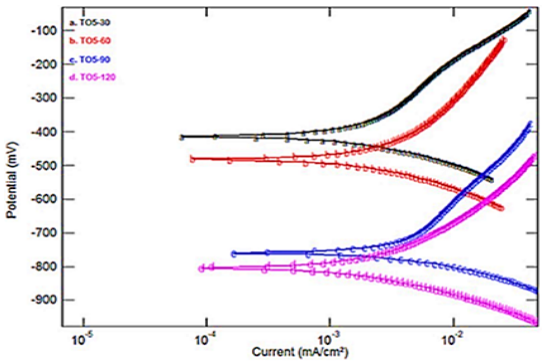

Fig. 27. Polarization curves of TO5 exposed under SW

Table 2: Corrosion kinetic parameters of specimens exposed under SW

System with Duration	E_{corr}(mV)	I_{corr}(mA/cm^2)	CR(mils/yr.)	IE(%)
BS-30	-642.33	0.1925204	87.84600	-
SC-30	-630.16	0.0051500	2.349900	97.32
CN1-30	-627.20	0.0023965	1.093500	98.76
CN3-30	-584.91	0.0022824	1.041400	98.81
CN5-30	-503.22	0.0014020	0.639721	99.27
TO1-30	-643.15	0.0014533	0.663143	99.25
TO3-30	-549.23	0.0012660	0.577668	99.34
TO5-30	-413.55	0.0015134	0.690554	99.21
BS-60	-659.01	0.8052888	367.4500	-
SC-60	-579.66	0.0077843	3.551900	99.03
CN1-60	-602.44	0.0028111	1.282600	99.65
CN3-60	-559.74	0.0027971	1.276200	99.66
CN5-60	-699.16	0.0018487	0.843562	99.77
TO1-60	-546.91	0.0034340	1.566900	99.57
TO3-60	-593.03	0.0028437	1.297500	99.64
TO5-60	-481.47	0.0022780	1.039400	99.72
BS-90	-730.85	0.9161511	418.0300	-
SC-90	-590.24	0.0102179	4.662400	98.88
CN1-90	-416.76	0.0087104	3.974500	99.05
CN3-90	-529.32	0.0055638	2.538700	99.39
CN5-90	-587.19	0.0037598	1.758600	99.58
TO1-90	-533.32	0.0040853	1.864100	99.55
TO3-90	-546.98	0.0036646	1.672100	99.60
TO5-90	-758.82	0.0028159	1.715600	99.59
BS-120	-746.24	1.9535000	891.4200	-
SC-120	-490.42	0.0124411	5.676800	99.36
CN1-120	-525.41	0.0101810	4.193400	99.53
CN3-120	-553.44	0.0065127	2.971700	99.67
CN5-120	-492.56	0.0053817	2.611900	99.71
TO1-120	-574.08	0.0068182	3.111100	99.65
TO3-120	-545.86	0.0044747	2.041800	99.77
TO5-120	-804.10	0.0036795	1.678900	99.81

All the coating systems show appreciable level of corrosion inhibition efficiency. For instance, IE of SC, CN5 and TO5 with respect to the BS, at the exposure duration of 30, 60, 90 and 120 days were found as 97.32%, 99.03%, 98.88% and 99.36%; 99.27%, 99.77%, 99.58% and 99.71%; 99.21%, 99.72 %, 99.69% and 99.81% respectively. It was observed that the incorporation of calcium nitrite and nano-TiO_2 significantly enhanced the inhibition efficiency of the plain cement slurry coating system. For example, the IE of CN5 with respect to the SC, at the exposure duration of 30, 60, 90 and 120 days were found as 72.78%, 76.25%, 62.28% and 53.99% respectively; the corrosion inhibition efficiency of TO5 with respect to the SC, at the exposure duration of 30, 60, 90 and 120 days were found as 70.61%, 70.74%, 63.20% and 70.43% respectively. Furthermore, the efficiency of CN5 and TO5 as compared to BS and SC after 120 days exposure can be evidently seen in the Figure 28.

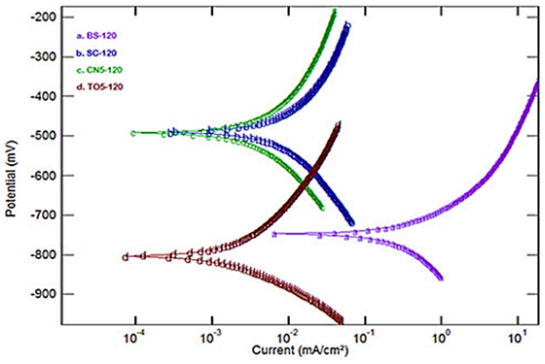

Fig. 28. Polarization curve of BS, SC, CN5 and TO5 systems exposed under saline water for 120 days

Weight Loss Measurements

The weight loss measurements of all the systems exposed in normal tap water as well as saline water for 120 days were carried out and then corrosion rate and inhibition efficiency were determined as given in Table 3. It was observed that the corrosion rate decreases as the amount of calcium nitrite and nano-TiO_2 increases in the coating system, thus inhibition efficiency increases with increasing the quantity of calcium nitrite and nano-TiO_2. For example, the corrosion inhibition efficiency of CN1, CN3 and CN5 exposed under saline water was found to be 99.57%, 99.67% and 99.72% with respect to the BS; 41.48%, 55.08% and 62.08% with respect to the SC respectively; and the corrosion inhibition efficiency of TO1, TO3 and TO5 exposed under saline water was found to be 99.63%, 99.68% and 99.76% with respect to the BS; 49.49%, 57.08% and 67.70% with respect to the SC respectively.

The results of this investigation revealed that the calcium nitrite and nano-TiO_2 admixed cement slurry coatings are more effective in corrosion of steel as compared to normal cement slurry coatings as investigated by earlier studies[22,23].

Table 3: Corrosion rate and inhibition efficiency of the systems after 120 days exposure using weight loss method

System with Duration	Systems Exposed Under Tap Water		Systems Exposed Under Saline Water	
	CR(mils/yr.)	IE(%)	CR(mils/yr.)	IE(%)
BS-120	5.7824	-	874.3246	-
SC-120	2.8135	51.34	6.4870	99.26
CN1-120	1.7432	69.85	3.7964	99.57
CN3-120	1.4841	74.33	2.9138	99.67
CN5-120	1.219	78.92	2.4596	99.72
TO1-120	1.3967	75.85	3.2765	99.63
TO3-120	1.2858	77.76	2.7840	99.68
TO5-120	1.1347	80.38	2.0955	99.76

Setting Time and Compressive Strength

The influences of calcium nitrite and nano-TiO_2 on the hardening process of cement pastes were assessed by determining the setting time as shown in Fig. 29. It was observed that the initial setting time was reduced by 10.9%, 17.4% and 23.9% when 1%, 3% and 5% calcium nitrite were added. This is due to the fact that the calcium nitrite acts as set accelerators, which also fulfill the ASTM C 494 requirements. Furthermore, the initial setting time was found to be decreased by 19.6%, 34.8% and 43.5% when 1%, 3% and 5% nano-TiO_2 were added. This is due to its (nano-TiO_2) seeding effect, nano-TiO_2 perform as seeds for the precipitation of the cement hydration products and thus accelerate the hydration process.

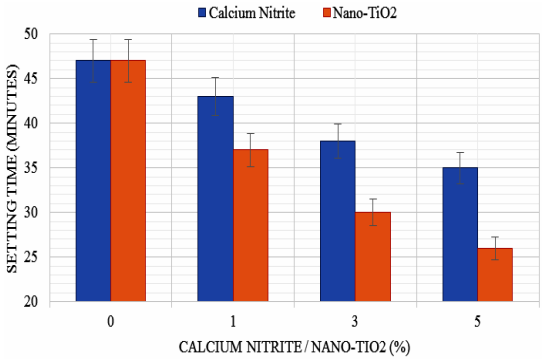

Fig. 29. Setting of cement paste containing calcium nitrite and nano-TiO_2

The 3, 7, and 28-days compressive strength of cement mortar containing calcium nitrite and nano-TiO_2 is given in Fig. 30. It was observed that the calcium nitrite admixed mortar showed the higher strength as compared to uninhibited specimens. Also, the compressive strength was found to be increased as the dosage of calcium nitrite increased. Thus, addition of calcium nitrite showed the enhanced strength which suggests that there is no adverse effect at early ages. This may be due to increased rate of hydration of cement with calcium nitrite at early ages. Further, the nano-TiO_2 incorporated cement mortar showed higher compressive strength at all the ages. Also, it has been observed that the strength was remarkably increased as the dosage of nano-TiO_2 increased, for instance the 28-day compressive strength of cement mortar containing 1%, 3% and 5% of nano-TiO_2 was found to be improved by 2.7%, 5.7% and 10.2% respectively as compared to control mortar. These enhancements are due to the fact that nano-TiO_2 acts as micro pore fillers and hydration process accelerators.

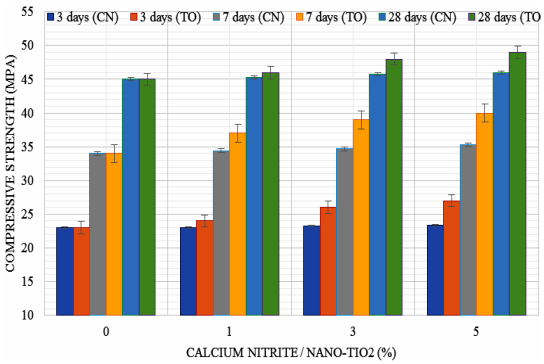

Fig. 30. Compressive strength of cement mortar containing calcium nitrite and nano-TiO_2

CONCLUSION

The performance of corrosion protective ordinary cement slurry coatings on steel with different contents of calcium nitrite and nano-TiO_2 was investigated. All coating systems were subjected to exposure in normal tap water and saline water for up to 120 days. Besides, to assess the influence of calcium nitrite and nano-TiO_2 on the quality of cementitious composite, setting time and compressive strength were determined. The following conclusions were obtained.

The corrosion rate of calcium nitrite incorporated cement slurry coated steel was found to be reduced with increasing the dosage of calcium nitrite. Thus, an increase in the amount of calcium nitrite, enhance the inhibition efficiency considerably, for instance the inhibition efficiency of CN1, CN3 and CN5 exposed under saline environment after 120 days with respect to the BS was found to be 99.53%, 99.67% and 99.71% respectively as calculated from potentiodynamic polarization measurements; 99.57%, 99.67% and 99.72% respectively as obtained from weight loss measurement. However, the inhibition efficiency with respect to the SC was found to be 26.13%, 47.65% and 53.99% respectively as calculated from potentiodynamic polarization measurements; 41.47%, 55.08% and 62.08% respectively as obtained from weight loss measurement.

The corrosion inhibition effect of nano-TiO_2 added cement slurry coated steel was remarkable.

The corrosion rate was found to be decreased by an increase in the dosage of nano-TiO_2, for example the inhibition efficiency of TO1, TO3 and TO5 exposed under saline environment after 120 days with respect to the BS was found to be 99.65%, 99.77% and 99.81% respectively as calculated from potentiodynamic polarization measurements; 99.63%, 99.68% and 99.76% respectively as obtained from weight loss measurement. Though, the inhibition efficiency relative to the SC was found to be 45.20%, 64.03%, and 70.43%, respectively, as calculated from potentiodynamic polarization measurements, and 49.49%, 57.08%, and 67.70%, respectively, as determined from weight loss measurements.

The initial setting time of cement was observed to be reduced by 10.9%, 17.4% and 23.9% when 1%, 3% and 5% calcium nitrite were added; and this decrement was found to be 19.6%, 34.8% and 43.5% when 1%, 3% and 5% nano-TiO_2 were incorporated.

The compressive strength was found to be enhanced as the dosage of calcium nitrite and nano-TiO_2 increased. For instance, the 28-day compressive strength of cement mortar containing 1%, 3% and 5% calcium nitrite as compared to control mortar was found to be improved by 1.36%, 2.27% and 4.08% respectively; however, this enhancement was found to be 2.7%, 5.7% and 10.2% when 1%, 3% and 5% nano-TiO2 were added.

ACKNOWLEDGMENT

This research did not receive any specific grant from funding agencies in the public, commercial, or not-for-profit sectors.

Conflict of interest

The author declare that we have no conflict of interest.

REFERENCES

1. Batis, G.; Routoulas, A.; Rakanta, E., *Cement Concr. Compos.*, **2003**, *25*, 109-115.
2. Ahmad, S., *Cement Concr. Compos.*, **2003**, *25*, 459-471.
3. Fajardo, G.; Valdez, P.; Pacheco, J., *Constr. Build. Mater.*, **2009**, *23*, 768-774.
4. Söylev, T. A.; Richardson, M. G., *Constr. Build. Mater.,* **2008**, *22*, 609-622.
5. Daniyal, M.; Akhtar, S., *J. Build. Pathol. Rehabil.*, **2020**, *5*, 1-20.
6. Liu, Q.; Leung Su, R. K.; Xu, F., *Constr. Build. Mater.*, **2021**, 297.
7. Robuschi, S.; Tengattini, A.; Dijkstra, J.; Fernandez, I.; Lundgren, K., *Cement Concr. Res.*, **2021**, 144.
8. Ji, Y.; Zhan, G.; Tan, Z.; Hu, Y.; Gao, F., *Constr. Build. Mater.*, **2015**, *79*, 214-222.
9. Ann, K. Y.; Jung, H. S.; Kim, H. S.; Kim, S. S.; Moon, H. Y., *Cement Concr. Res.*, **2006**, *36*, 530-535.
10. Zomorodian, A.; Behnood, A., *Buildings.*, **2023**, *13*, 1-20.
11. Ramirez, A. M.; De Belie, N., *RILEM State Art Rep.*, **2011**, *5*, 11-15.
12. Daniyal, M.; Azam, A.; Akhtar, S., *Adv. Struct. Mater.*, **2018**, *84*, 169-189.
13. Janczarek, M.; Klapiszewski, Ł.; Jędrzejczak, P.; Klapiszewska, I.; Łosarczyk, A.; Jesionowski, T., *Chem. Eng. J.*, **2022**, 430.
14. Daniyal, M.; Akhtar, S.; Azam, A.; Islam, S., *Arab J. Sci. Eng.*, **2020**, *45*, 4369-4385.
15. Li, Z.; Ding, S.; Yu, X.; Han, B.; Ou, J., *Compos. Part A: Appl. Sci. Manuf.,* **2018**, *111*, 115-135.
16. Daniyal, M.; Akhtar, S.; Azam, A.; Islam, S., *Sādhan.*, **2020**, *45*, 1-14.
17. Umoren, S. A.; Solomon, M. M.; Saji, V. S., *Polymeric Mater. Corros. Inhib.*, **2022**, *4*, 103-127.
18. Daniyal, M.; Akhtar, S.; Azam, A., *J. Mater. Res. Technol.*, **2019**, *8*, 6158-6172.
19. Speight, J. G., *Oil Gas Corros. Prev.*, **2014**, *6*, 109-149.
20. ASTM G1-90, *Standard Practice Preparing Cleaning Evaluating Corrosion Test Specimens.*, **1999**, 1-8.
21. Ibrahimi, B.; Berdimurodov, E., *Electrochem. Anal. Tech. Sustain. Corros. Monit.*, **2023**, *5*, 81-90.
22. Vedalakshmi, R.; Kumar, K.; Raju, V.; Rengaswamy, N. S., *Cem. Concr. Compos.,* **2000**, *22*(6), 417-421.
23. Pei, X.; Noël, M.; Green, M.; Fam, A.; Shier, G., *Surf. Coat. Technol.*, **2017**, *315*, 188-195.